

THE SPECTRAL ENERGY DISTRIBUTIONS OF $Z \sim 8$ GALAXIES FROM THE IRAC ULTRA DEEP FIELDS: EMISSION LINES, STELLAR MASSES, AND SPECIFIC STAR FORMATION RATES AT 650 MYR ¹

I. LABBÉ², P. A. OESCH^{3,4}, R. J. BOUWENS², G. D. ILLINGWORTH³, D. MAGEE³, V. GONZÁLEZ³, C. M. CAROLLO⁵, M. FRANX², M. TRENTI⁶, P. G. VAN DOKKUM⁷, M. STIAVELLI⁸

Draft version October 28, 2021

ABSTRACT

Using new ultra-deep Spitzer/IRAC photometry from the IRAC Ultra-deep Field program (IUDF), we investigate the stellar populations of a sample of 63 Y -dropout galaxy candidates at $z \sim 8$, only 650 Myr after the Big Bang. The sources are selected from HST/ACS+WFC3/IR data over the Hubble Ultra Deep Field (HUDF), two HUDF parallel fields, and wide area data over the CANDELS/GOODS-South. The new Spitzer/IRAC data increase the coverage in [3.6] and [4.5] to ~ 120 h over the HUDF reaching depths of ~ 28 (AB, 1σ). The improved depth and inclusion of brighter candidates result in direct $\geq 3\sigma$ IRAC detections of 20/63 sources, of which 11/63 are detected at $\geq 5\sigma$. The average [3.6] – [4.5] colors of IRAC detected galaxies at $z \sim 8$ are markedly redder than those at $z \sim 7$, observed only 130 Myr later. The simplest explanation is that we witness strong rest-frame optical emission lines (in particular [O III] $\lambda\lambda 4959, 5007 + H\beta$) moving through the IRAC bandpasses with redshift. Assuming that the average rest-frame spectrum is the same at both $z \sim 7$ and $z \sim 8$ we estimate a rest-frame equivalent width of $W_{[OIII]\lambda\lambda 4959, 5007 + H\beta} = 670_{-170}^{+260}$ Å contributing $0.56_{-0.11}^{+0.16}$ mag to the [4.5] filter at $z \sim 8$. The corresponding $W_{H\alpha} = 430_{-110}^{+160}$ Å implies an average specific star formation rate of $sSFR = 11_{-5}^{+11}$ Gyr⁻¹ and a stellar population age of 100_{-50}^{+100} Myr. Correcting the spectral energy distribution for the contribution of emission lines lowers the average best-fit stellar masses and mass-to-light ratios by $\sim 3\times$, decreasing the integrated stellar mass density to $\rho^*(z=8, M_{UV} < -18) = 0.6_{-0.3}^{+0.4} \times 10^6 M_{\odot} \text{ Mpc}^{-3}$.

Subject headings: galaxies: evolution — galaxies: high-redshift

1. INTRODUCTION

Deep imaging of high redshift $z > 6$ galaxies at mid-infrared wavelengths with the InfraRed Array Camera (IRAC; Fazio et al. 2004) on *Spitzer* has led to the surprising discovery that $z \geq 6$ galaxies have red $H - [3.6] \sim 0.5$ colors. This has been taken as evidence of substantial stellar masses $\sim 10^9 - 10^{10} M_{\odot}$ (Eyles et al. 2005; Yan et al. 2006; Stark et al. 2009) and stellar ages (> 300 Myr) (Labbé et al. 2006; González et al. 2010;

Labbé et al. 2010a,b). Early studies also suggested that the specific star formation rate at fixed stellar mass was nearly flat at $3 < z < 8$, in apparent disagreement with the strongly increasing specific inflow rates of baryons predicted by galaxy formation models (e.g., Neistein & Dekel 2008; Davé et al. 2011; Weinmann et al. 2011).

A key uncertainty in the analysis of the photometry is how much rest-frame optical emission lines contribute to the broadband fluxes. If emission lines are very strong, then the stellar masses previously derived by fitting stellar population models without lines would be biased high, and the specific star formation rate (sSFR) would be biased low (e.g., Labbé et al. 2010b, Schaerer & de Barros 2010). To address this issue, emission lines have been included in some stellar population models (e.g., Schaerer et al. 2010, 2012, de Barros et al. 2012, Yan et al. 2012). As model predictions for emission lines are very uncertain empirical approaches are complementary and necessary.

Fumagalli et al. (2012) studied the evolution of the $H\alpha$ equivalent width at $0 < z < 2$ using near-IR spectra and predict very large values at $z \sim 8$. If the emission lines are indeed as strong as argued, then deep photometry should be able to reveal the effect of the lines moving through the IRAC passbands with redshift. This technique has been applied successfully by looking for excess flux in the [3.6]–band due to $H\alpha$ at $z \sim 4.5$ (e.g. Shim et al. 2011, Stark et al. 2013) and by comparing the average observed IRAC colors over $4 < z < 6$ (Gonzalez et al. 2012). Nevertheless, the current situation is that the contribution of emission lines at $4 < z < 8$ is still poorly known.

¹ Based on observations made with the NASA/ESA Hubble Space Telescope, which is operated by the Association of Universities for Research in Astronomy, Inc., under NASA contract NAS 5-26555. These observations are associated with programs #11563, 9797. Based on observations with the Spitzer Space Telescope, which is operated by the Jet Propulsion Laboratory, California Institute of Technology under NASA contract 1407. Support for this work was provided by NASA through contract 125790 issued by JPL/Caltech. Based on service mode observations collected at the European Southern Observatory, Paranal, Chile (ESO Program 073.A-0764A). Based on data gathered with the 6.5 meter Magellan Telescopes located at Las Campanas Observatory, Chile.

² Leiden Observatory, Leiden University, NL-2300 RA Leiden, Netherlands

³ UCO/Lick Observatory, University of California, Santa Cruz, CA 95064

⁴ Hubble Fellow

⁵ Institute for Astronomy, ETH Zurich, 8092 Zurich, Switzerland

⁶ Kavli Institute for Cosmology and Institute of Astronomy, University of Cambridge, United Kingdom

⁷ Department of Astronomy, Yale University, New Haven, CT 06520

⁸ Space Telescope Science Institute, Baltimore, MD 21218, United States

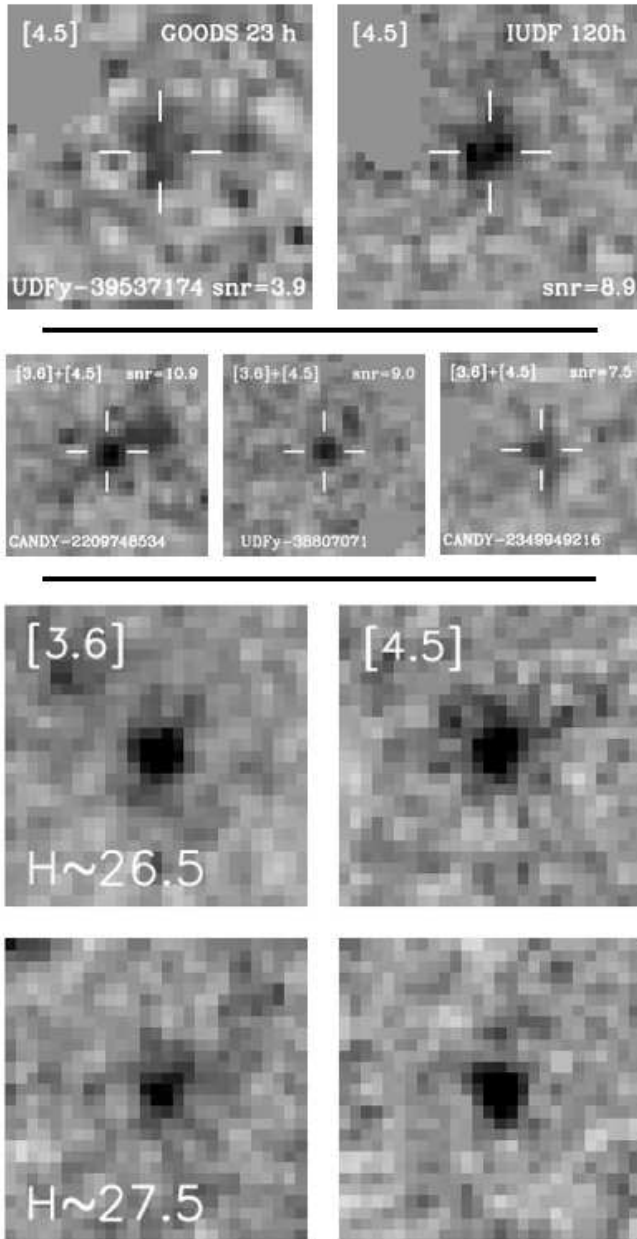


Figure 1. (*top panels*) A comparison of Spitzer/IRAC [4.5] band images between GOODS (23h exposure time) and the new IUDF observations (120h) for Y_{105} -dropout galaxy UDFy-3953714 (Bouwens et al. 2011a) at $z \sim 8$. Nearby foreground sources have been subtracted. With the new IUDF IRAC data the object is clearly detected, even in the shallower IRAC [4.5] micron band. (*middle panels*) Summed [3.6]+[4.5] micron images of several IRAC detected Y_{105} -dropouts from our sample. (*bottom panels*) Median stacked IRAC images of $z \sim 8$ Y -dropout sources, grouped in ~ 1 -mag bins centered on $H_{160} \approx 26.5, 27.5$, containing 10 and 23 galaxies, respectively. Importantly, the stacks show significant detections at [3.6], which at $z \sim 8$ is only moderately affected by emission lines. Image panels are shown in inverted grayscale and are $10'' \times 10''$.

Direct estimates at $z \sim 8$ would provide the best constraints yet on the evolution of emission line strengths and specific star formation rate to the highest redshifts. Fortunately, at redshift $z \sim 8$ a relatively clean test is possible for the strength of the strongest lines [O III] $\lambda\lambda 4959, 5007+H\beta$, because these lie isolated in the

[4.5] filter. Then main challenge is the extreme faintness of the sources.

In this Letter, we use the largest sample of $z \sim 8$ galaxy candidates in combination with newly acquired ultra-deep IRAC data from the IRAC Ultra Deep Field program (IUDF; PI Labbé) to study their colors, SEDs, the contribution of emission lines, and to derive emission line corrected stellar masses and specific star formation rates. Throughout this paper, we assume an $\Omega_M = 0.3, \Omega_\Lambda = 0.7$ cosmology with $H_0 = 70 \text{ km s}^{-1} \text{ Mpc}^{-1}$. Magnitudes are in the AB photometric system (Oke & Gunn 1983).

2. DATA

The data analyzed here consist of ultra-deep WFC3/IR imaging from the HUDF09 program (GO 11563: PI Illingworth) over the HUDF and two nearby fields HUDF09-1 and HUDF09-2, supplemented with deep WFC3/IR data observations from the Early Release Science program (GO 11359: PI O’Connell) and the Multi-Cycle Treasury program CANDELS (PI: Faber/Ferguson; Grogin et al. 2011; Koekemoer et al. 2011) over the GOODS-South.

We use new ultra-deep Spitzer/IRAC imaging from the IRAC Ultra-deep Field program (IUDF; PI Labbé, PID 70145), a 262 hour Spitzer warm mission program at [3.6] and [4.5] micron (Labbé et al. in preparation). This survey increases the exposure time over the HUDF, HUDF09-1 and HUDF09-2 fields from 12 – 46 hours to ~ 120 hours, ~ 50 hours, and 80 – 120 hours, respectively. For the wider GOODS area we use the 23–46 hour deep IRAC coverage of GOODS (M. Dickinson et al. in preparation).

Our primary sample consists of 60 Y -dropout galaxies at $z \sim 8$ selected by Bouwens et al. (2011a) over the HUDF09 and ERS fields and 16 brighter Y -dropouts selected by Oesch et al. (2012) over the CANDELS GOODS-South area.⁹

We derive new IRAC photometry of all 76 sources following the procedure of Labbé et al. (2010a,b). Briefly, we subtract nearby foreground sources based on their HST image profiles and determine local backgrounds (see e.g. Gonzalez et al 2011). Then we perform aperture photometry through $2''$ diameter apertures on the cleaned images and correct the flux for light outside the aperture using a profile derived from nearby stars ($2.4\times$ in [3.6] and $2.5\times$ in [4.5]). Details of the photometry are presented in Labbé et al. (in preparation). We exclude 13 sources for which clean subtraction was not possible due to the proximity of very bright foreground sources, leaving a final sample of 63 Y -dropouts.

Figure 1 presents image stamps of IRAC-detected Y -dropout galaxies. A direct comparison to earlier GOODS observations demonstrates the clear improvement in sensitivity with the new IRAC Ultra-deep Field data.

We also include fainter, IRAC undetected, galaxies in the analysis by stacking $15'' \times 15''$ image stamps centered on the sources. On the stacks we subtract any residual background in a concentric annulus $5'' < r < 7.5''$.

⁹ The ERS data uses the Y_{098} filter versus the Y_{105} filter in CANDELS+HUDF. However, the criteria from Bouwens et al. 2011 and Oesch et al 2012 were chosen in such a way that the samples would have a very similar redshift distribution.

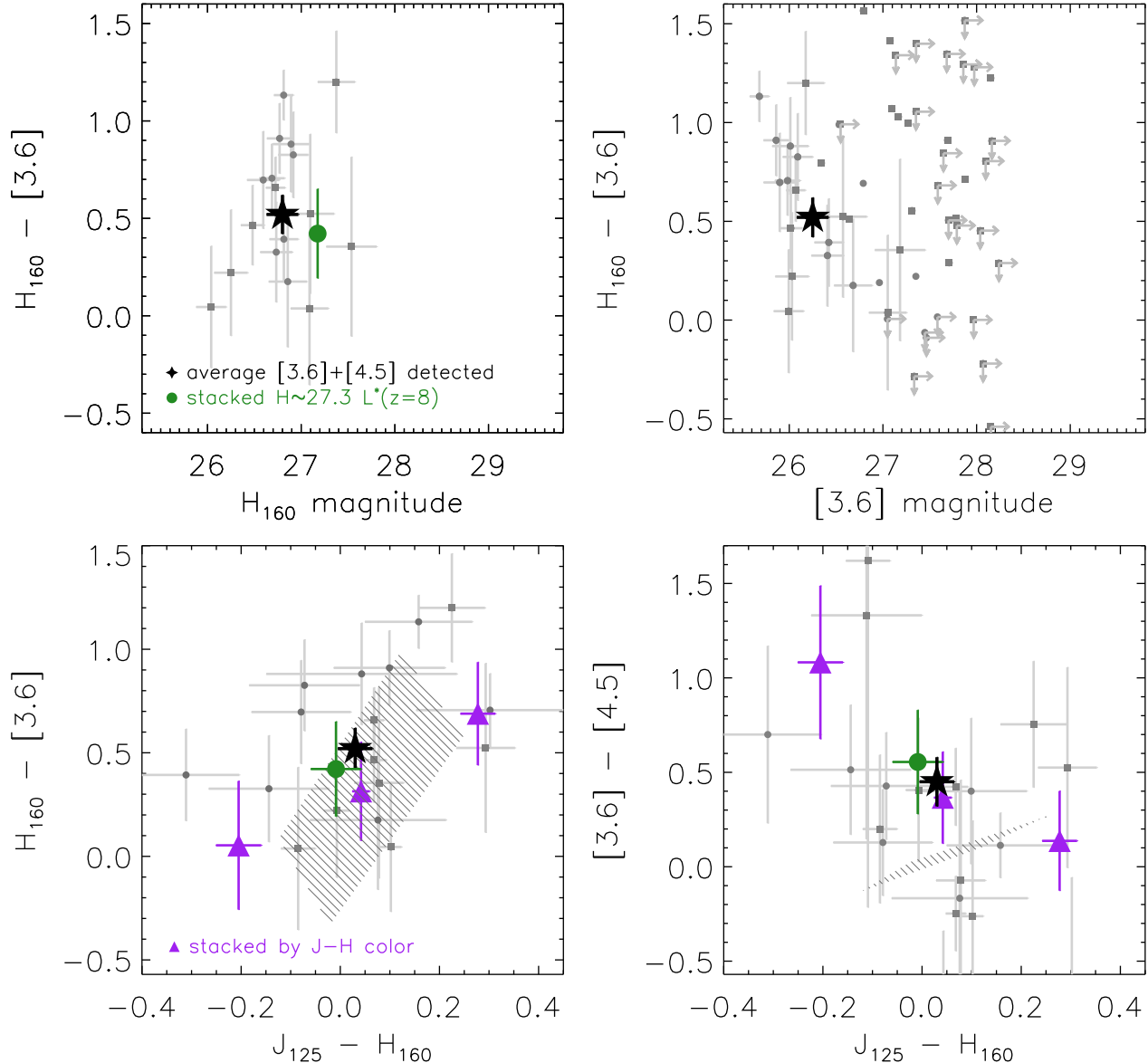


Figure 2. A first exploration of the observed IRAC properties of $z \sim 8$ galaxies in our fields. Galaxies directly detected at $> 3\sigma$ in IRAC bands [3.6] + [4.5] are shown by gray points (squares for ultra-deep IRAC from IUDF, circles for wide-field IRAC from GOODS). The averages of IRAC detected galaxies are indicated by filled stars. Stacked measurements in a 1-magnitude bin centered at $H = 27.3$ ($\sim L_{UV}^*(z = 8)$), including IRAC undetected sources, are shown in green. Stacking measurements of $H \leq 28$ galaxies in bins of $J_{125} - H_{160}$ colors are shown in purple. *Top left panel:* the $H_{160} - [3.6]$ versus H_{160} diagram. *Top right panel:* the observed $H - [3.6]$ versus [3.6] magnitude. Sources with $\text{SNR}([3.6] + [4.5]) < 3\sigma$ are also shown (upper limits are 1σ in [3.6]). The deepest data over the HUDF reach [3.6] ~ 28 mag AB (1σ). *Lower left panel:* the observed $H - [3.6]$ versus $J_{125} - H_{160}$ is in the range predicted by dust-reddened Bruzual & Charlot (2003, BC03) stellar population synthesis models, with some evidence for a correlation of $H - [3.6]$ with $J_{125} - H_{160}$. The hatched region shows models with a formation redshift $z = 10$ in the redshift range $7.3 < z < 8.3$ and with Calzetti et al. (2000) reddening $E(B - V) < 0.2$. *Lower right panel:* in contrast, the observed [3.6] - [4.5] colors are on average ~ 0.5 mag redder than the BC03 models (rest-frame $B_{4000} - V_{5000}$), in particular at bluer $J_{125} - H_{160}$ colors. Likely, the [4.5] flux is boosted by the contribution of the emission lines [O III] $\lambda\lambda 4959, 5007$ and $H\beta$.

We compare between average and median combination to make sure that average results are not driven by outliers and derive uncertainties by bootstrap resampling.

3. OBSERVED PROPERTIES

To explore the observed properties of $z \sim 8$ galaxies, we first present color-magnitude and color-color diagrams which contain diagnostic information about their stellar populations. Figure 2 (*left panel*) shows the $H_{160} - [3.6]$ versus H_{160} color-magnitude diagram. The

improved IRAC depth and inclusion of brighter candidates result in a direct detection with signal-to-noise ratio $\text{SNR}([3.6] + [4.5]) \geq 3$ of 20/63 sources (32%), of which 11 (17%) are detected at $\geq 5\sigma$.

The average colors of IRAC detected ($\geq 3\sigma$) galaxies are $\langle H - [3.6] \rangle = 0.52 \pm 0.09$, with an intrinsic scatter of $\sigma(H - [3.6]) = 0.40 \pm 0.12$ (photometric uncertainties subtracted in quadrature), and $\langle [3.6] - [4.5] \rangle = 0.43 \pm 0.11$ with $\sigma(H - [3.6]) = 0.55 \pm 0.15$. Stacking fainter $H \sim 27.3$ ($\sim L^*(z = 8)$) galaxies, including IRAC undetected

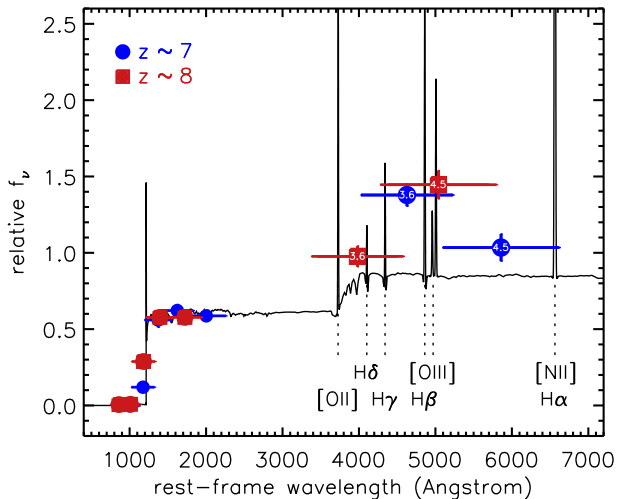


Figure 3. A comparison of the average rest-frame SEDs of IRAC detected galaxies at $z \sim 7$ and $z \sim 8$ from the average HST/ACS, HST/WFC3, and Spitzer/IRAC fluxes. The IRAC [3.6] and [4.5] fluxes are indicated. The SEDs are in units of $f\nu$ (arbitrary scaling). A young star forming stellar population model with emission lines is shown in black. The observed [3.6] – [4.5] colors at $z \sim 7$ and $z \sim 8$ are substantially different, despite the short time elapsed between these epochs (about 130Myr). Combined, the rest-frame SEDs suggest a clear flux excess at $\sim 5000\text{\AA}$, shifting from [3.6] at $z \sim 7$ to [4.5] at $z \sim 8$, likely due to a contribution from strong [O III] $_{\lambda 4959, 5007}$ and $H\beta$ emission lines.

sources, shows similar colors. The mean $\langle H - [3.6] \rangle$ color is in the range of predictions from dust reddened Bruzual & Charlot (2003, BC03) stellar population synthesis models, but the $\langle [3.6] - [4.5] \rangle$ appears significantly redder by ~ 0.5 mag.

No obvious trend of $H_{160} - [3.6]$ color with H_{160} or [3.6] magnitude is seen, but the $H_{160} - [3.6]$ (rest-frame $U_{1700} - B_{4000}$ at $z \sim 8$) does appear to correlate (at $\sim 2\sigma$ confidence) with $J_{125} - H_{160}$ colors consistent with expectations from dust reddened BC03 stellar population models. The trend is seen both in IRAC detected galaxies and in $H_{160} \leq 28$ selected samples ($\leq 0.3L^*$ ($z = 8$)), including IRAC undetected galaxies. In contrast, the observed [3.6] – [4.5] colors (rest-frame $B_{4000} - V_{5000}$) are generally redder than the BC03 models, with larger offsets at bluer $J_{125} - H_{160}$ colors.

Figure 3 shows the average spectral energy distributions of IRAC detected galaxies at $z \sim 8$ compared those at $z \sim 7$, only 130Myr later. It is obvious that the observed [3.6] – [4.5] colors are markedly different. Shifted to the rest-frame, the SEDs viewed together suggest a clear flux excess at $\sim 5000\text{\AA}$, shifting from [3.6] at $z \sim 7$ to [4.5] at $z \sim 8$. The excess is likely caused by [O III] $_{\lambda 4959, 5007}$ and $H\beta$ emission lines, which are expected to be strong in young star forming galaxies at low metallicities (e.g., Schaerer et al. 2010).

Nevertheless, it is difficult to determine the emission line contribution using stellar population model fits to the broadband photometry at each redshift separately. Degeneracies between age and dust in the model colors and systematic uncertainties in implementation of emission lines hamper such a direct solution. Instead, we will attempt to circumvent this limitation by using the joint

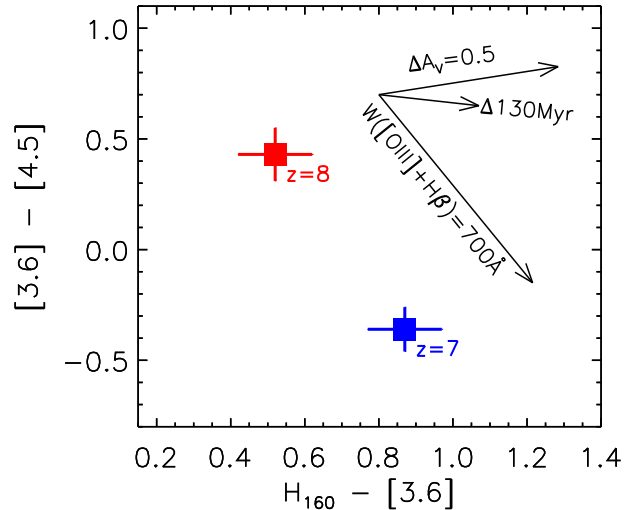


Figure 4. The $H - [3.6]$ versus $[3.6] - [4.5]$ colors of our samples of $z \sim 7$ and $z \sim 8$ galaxies. The [3.6] – [4.5] becomes ≈ 0.8 mag bluer from $z \sim 8$ to $z \sim 7$ while the $H - [3.6]$ colors become ≈ 0.4 mag redder. The arrows show the effect of 1) increasing dust obscuration by $\Delta A_V = 0.5$ between the two epochs, 2) changing the stellar population age by 130Myr (assuming CSF since $z = 10$), and 3) strong [O III] $_{\lambda 4959, 5007} + H\beta$ emission moving from [4.5] at $z \sim 8$ into [3.6] at $z \sim 7$. Emission lines provide the most probable explanation for the observed change.

SED information at the two adjacent redshifts to isolate the effective emission line contribution.

4. REST-FRAME OPTICAL EMISSION LINES

Figure 4 shows clearly that the observed [3.6] – [4.5] colors at $z \sim 8$ are 0.8 mag redder compared to $z \sim 7$, while the $H - [3.6]$ colors are 0.4 mag bluer¹⁰. Changes in stellar population age and/or dust can not produce such differences, but strong optical emission lines naturally reproduce the observed change.

With the reasonable assumption that the average rest-frame spectrum is the same at both $z \sim 8$ and $z \sim 7$, we can solve directly for the rest-frame equivalent width of these emission lines.

Considering only [O III] $_{\lambda 4959, 5007}$ and $H\beta$ and applying the redshift selection functions of Oesch et al. (2012) and Bouwens et al. (2011a), a linear fit to the colors produces $W_{[\text{O III}]_{\lambda 4959, 5007} + H\beta} = 500\text{\AA}$. The redshift distribution accounts for the fact that emission lines may contribute to both [3.6] and [4.5]. Using the tabulated emission line values of Anders & Fritze-v. Alvensleben (2003) for sub-Solar metallicity $0.2Z_{\odot}$ (Erb et al. 2006; Maiolino et al. 2008), we also correct for the smaller integrated contributions of $H\alpha$, $H\beta$, $H\gamma$, [N II] and [O II], leading to $W_{[\text{O III}]_{\lambda 4959, 5007} + H\beta} = 670\text{\AA}$.

Note that this estimate is to first order independent of stellar population models and the fit only has one free parameter: the combined rest-frame equivalent width of the strong emission lines. The main systematic uncertainty is the redshift selection function for the $z \sim 7$ sample, as the [O III] line moves from the [3.6] to the

¹⁰ Note, the samples are similar in brightness, $H \sim 26.8$ for $z \sim 8$ and $H \sim 26.5$ for $z \sim 7$, hence both $\sim 1.5L^*(UV)$ in luminosity at $z \sim 8$ and $z \sim 7$ respectively.

[4.5] filter at $z > 7.0$. A secondary uncertainty is the effect of metallicity, which changes the emission line ratios. To evaluate the impact of both effects we shift the central redshift of the $z \sim 7$ distribution by up to $\Delta z = 0.3$ in either direction and vary the metallicity from $0.2 - 1.0 Z_{\odot}$. We add these systematic uncertainties in quadrature to the photometric errors arriving at $W_{[OIII]\lambda\lambda 4959,5007+H\beta} = 670_{-170}^{+260} \text{\AA}^{11}$.

The rest-frame equivalent width implies a boost of $0.55_{-0.11}^{+0.16}$ mag to [4.5] and smaller $0.19_{-0.09}^{+0.10}$ mag to [3.6] at $z \sim 8$, meaning the color of the stellar continuum is $[3.6] - [4.5] \approx 0$. Using the line ratios of Anders & Fritzev-Alvensleben (2003) for a metallicity of $0.2 Z_{\odot}$ and taking into account the slope of the continuum ($f_{\nu} \approx \text{constant}$ or $f_{\lambda} \propto \lambda^{-2}$) the corresponding $H\alpha$ equivalent is $W_{H\alpha} = 430_{-110}^{+160}$. Note that the inferred $WH\alpha$ depends on assuming line ratios.

5. SPECIFIC STAR FORMATION RATES AND STELLAR MASSES

A common approach to estimate the sSFR is derive it from $W_{H\alpha}$, using the $H\alpha$ to SFR conversion of Kennicutt (1998) and the stellar continuum from BC03 stellar populations synthesis models. The model adopts a Salpeter (1955) initial mass function (IMF) between $0.1 - 100 M_{\odot}$, a metallicity of $0.2 Z_{\odot}$, and constant star formation rate. Using the indirect estimate of $H\alpha$ we derive $sSFR = 11_{-5}^{+11} \text{ Gyr}^{-1}$, corresponding to an approximate stellar age of $100_{-50}^{+100} \text{ Myr}$. The estimated sSFR is not very sensitive to the assumed star formation history (e.g., declining and rising SFH introduce changes < 0.1 dex), but potentially significant uncertainties are the intrinsic line ratios, the possibly larger attenuation of the emission lines compared to the continuum and the escape fraction of ionizing photons. Larger attenuation and a non-zero escape fraction would increase the derived sSFR.

Fitting BC03 models with CSF to the broadband SEDs, we inspect the stellar masses and mass-to-light ratios after correcting the IRAC [3.6] and [4.5] bands for emission line contributions. The derived mass-to-light ratios of IRAC detected galaxies at $z \sim 8$ are $M/L_{1800} \approx 0.05$ and $M/L_V = 0.09$, in good agreement with those found by Yan et al. (2012) for two bright $z \sim 8$ sources. The M/L would have been overestimated by $\sim 3\times$ if emission lines had not been corrected. The scatter in M/L , based on the intrinsic scatter in $H - [3.6]$ and assuming CSF, is $\sigma(M/L_{1800}) = 0.25$ dex and $\sigma(M/L_V) = 0.1$ dex, where the luminosities refer to the stellar continuum only. This is likely a lower bound to the true scatter in M/L due to selection effects. The typical $L^*(UV, z = 8)$ galaxy (corresponding to $H \sim 27.3$) has a median rest-frame color $U - V \sim 0.2$ (stellar continuum only) and a stellar mass $M = 0.9_{-0.4}^{+0.6} \times 10^9 M_{\odot}$.

Model fits to the corrected SEDs can also be used to determine sSFRs, although these are rather uncertain due to the degeneracies between age and dust and the weak constraints on the UV-slope β at $z \sim 8$ (Bouwens et al.

2013). To mitigate the difficulties somewhat, we can fix the reddening to $A_V = 0.40 \pm 0.15$, consistent with the average β values of bright $z \sim 7$ galaxies (Bouwens et al. 2013). The best-fit sSFR is then $sSFR = 7_{-4}^{+13} \text{ Gyr}^{-1}$, in good agreement with the sSFR derived from $W_{H\alpha}$.

We derive integrated stellar mass densities of H -band selected galaxies to faint UV-limits by converting the stepwise UV -luminosity function (Bouwens et al. 2011a; Oesch et al. 2012) to stepwise mass densities, using the best-fit M/L to the emission line corrected SED.

Note that the emission line correction is derived from $\sim 1.5 L^*(UV, z = 8)$ galaxies, so we assume that the effect of emission lines is similar for $L < L^*$ galaxies. This approximation is unavoidable as sub- L^* galaxies are currently beyond the reach of Spitzer, even at our ultra-deep limits. We derive uncertainties by randomly drawing 10^4 LFs, perturbing the stepwise LF and M/L ratios by their errors, and integrating the resulting mass densities. Integrating to $M_{UV,AB} = -18$ yields $\rho^*(z = 8) = 0.6_{-0.3}^{+0.4} \times 10^6 M_{\odot} \text{ Mpc}^{-3}$.

6. DISCUSSION

This paper presents new ultra-deep IRAC data from the IUDF program (120 hours in [3.6] and [4.5] over the HUDF) in combination with a large sample of 63 Y_{105} -dropout galaxies at $z \sim 8$ to study average HST/WFC3 and Spitzer/IRAC SEDs, the effect of emission lines, and their impact on stellar population model fits.

The most exciting result is the direct detection of large numbers of $z \sim 8$ galaxies by Spitzer/IRAC to faint limits, without signs of a hard ‘‘confusion limit’’. The ability, for the first time, to determine the distribution of rest-frame optical colors at $z \sim 8$ is a clear reminder of the enduring capabilities of Spitzer, currently in its post cryogenic (‘‘warm’’) mission.

Using the joint IRAC constraints on the SED at $z \sim 7$ and $z \sim 8$, we derive an empirical constraint on the emission line contribution of rest-frame EW $W_{[OIII]\lambda\lambda 4959,5007+H\beta} \sim 670 \text{\AA}$ contributing ~ 0.5 mag to [4.5] at $z \sim 8$. To place this in context, we compare to recent estimates for star forming galaxies from other surveys (shown in Figure 5). While direct comparisons are difficult due to different techniques and stellar mass ranges, our results confirm the picture of an increasing importance of emission lines towards higher redshift (e.g., Shim et al. 2011, Fumagalli et al. 2012, Stark et al. 2013). The evolution of the rest-frame equivalent width of $H\alpha$ follows $W_{H\alpha} \propto (1+z)^{1.2 \pm 0.25}$ over $1 < z < 8$. This is a factor of ~ 2 slower than the power law derived by Fumagalli et al. (2012) over $0 < z < 2$, but in agreement with their model which assumes that the cumulative number density of progenitors at higher redshift remains constant (e.g., Dokkum et al. 2010, Papovich et al. 2011).

Clearly, at such high equivalent widths emission lines cannot be ignored when deriving stellar masses and ages at high redshift (e.g., Schaerer & de Barros 2010; de Barros et al. 2012). After correcting the SEDs for emission lines we find that the $L^*(z = 8)$ galaxies have stellar masses and M/L that are $\sim 3\times$ lower.

{The $W_{H\alpha}$ based sSFR = $11_{-5}^{+11} \text{ Gyr}^{-1}$ are $\sim 5\times$ higher than those at $z = 2$ (Reddy et al. 2012), consistent with

¹¹ Repeating the calculation using a fainter $26.8 < H < 27.8$ selected subsample, targeting galaxies around $L^*(z = 8)$ (Oesch et al. 2012), yields a similar value $W_{[OIII]\lambda\lambda 4959,5007+H\beta} = 560_{-170}^{+230} \text{\AA}$.

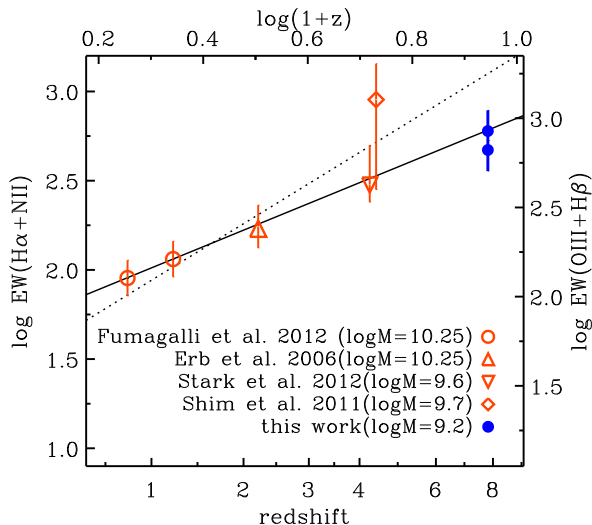


Figure 5. Comparison of the rest-frame emission line EW of star forming galaxies with redshift. Red points indicate estimates of the mean $H\alpha + [\text{NII}]$ EW with redshift, using either near-infrared spectra (Fumagalli et al. 2012, Erb et al. 2006) or emission line strengths inferred from excess emission in the IRAC [3.6] filter of spectroscopically confirmed galaxies at $z \sim 4 - 5$. The broadband derived $[\text{OIII}] + H\beta$ EW at $z \sim 8$ from this paper are shown by the blue solid symbols. They are placed on the same scale assuming the relative emission line strengths of Anders & Fritze-v. Alvensleben (2003) for sub-Solar $0.2Z_{\odot}$ (lower value) and Solar (higher value). The dotted line shows the EW evolution $\propto (1+z)^{1.8}$ derived by Fumagalli et al. (2012) for star forming galaxies with stellar mass $10.0 < \log(M/M_{\odot}) < 10.5$ at $0 < z < 2$ extrapolated to $z = 8$. The $z \sim 8$ point provides additional evidence for an increasing contribution of emission lines towards higher redshifts. The solid line shows the best-fit linear relation to all data at $1 < z < 8$: $W_{H\alpha} \propto (1+z)^{1.2 \pm 0.25}$.

an increase $sSFR \propto (1+z)^{1.5^{+0.7}_{-0.5}}$ between $2 < z < 8$. This evolution is somewhat higher than derived by Gonzalez et al. (2013) over $2 < z < 6$ and somewhat lower than inferred by Stark et al. (2013) at $2 < z < 7$, while in general agreement with the cumulative number density model of Fumagalli et al. 2012. The latest estimates reduce the tension between the observations and simulations, which predicted an evolution of the baryonic mass inflow rates $\propto (1+z)^{2.3}$ (e.g., Neistein & Dekel 2008; Davé et al. 2011, Weinmann et al. 2011).

Obviously, a huge leap in the determination of the properties of galaxies at these redshifts will be made possible by the arrival of JWST. But in the mean time wider and still deeper future IRAC observations will continue to provide valuable insight into the properties of the $z \sim 8$ population, with emerging detections of $z = 9 - 10$ (e.g., Zheng et al. 2012) galaxies probably not far behind.

We are grateful to Jarle Brinchmann, Steve Finkelstein, Casey Papovich, Dan Stark, Simone Weinmann for helpful discussions. We thank the anonymous referee for useful suggestions which improved the paper. Support

for this work was provided by NASA through Hubble Fellowship grant HF-51278.01. Support for this work was provided by NASA through an award issued by JPL/Caltech. This work has further been supported by NASA grant HST-GO-11563.01. We also acknowledge funding from ERC grant HIGHZ no. 227749.

Facilities: Spitzer (IRAC), HST (WFC3/IR)

REFERENCES

- Anders, P., & Fritze-v. Alvensleben, U. 2003, *A&A*, 401, 1063
 Bouwens, R. J., Illingworth, G. D., Franx, M., & Ford, H. 2008, *ApJ*, 686, 230
 Bouwens, R. J., et al. 2010, *ApJ*, 709, L133
 Bouwens, R. J., et al. 2010, *ApJ*, 708, L69
 —. 2011, *ApJ*, 737, 90
 Bouwens, R. J., Illingworth, G. D., Oesch, P. A., et al. 2012, *ApJ*, 754, 83
 Bouwens, R. J., Illingworth, G. D., Oesch, P. A., et al. 2012, *ApJ*, 754, 83
 Bouwens, R. J., Illingworth, G. D., Oesch, P. A., et al. 2013, *arXiv:1306.2950*
 Bruzual, G. & Charlot, S. 2003, *MNRAS*, 344, 1000 (BC03)
 Calzetti, D., et al. 2000, *ApJ*, 533, 682
 Davé, R. 2008, *MNRAS*, 385, 147
 de Barros, S., Schaerer, D., & Stark, D. P. 2012, *arXiv:1207.3663*
 Erb, D. K., Shapley, A. E., Pettini, M., Steidel, C. C., Reddy, N. A., & Adelberger, K. L. 2006, *ApJ*, 644, 813
 Eyles, L. P., et al. 2005, *MNRAS*, 364, 443
 Fazio, G. G., et al. 2004, *ApJS*, 154, 10
 Fumagalli, M., Patel, S., Franx, M., et al. 2012, *arXiv:1206.2645*
 González, V., Labbé, I., Bouwens, R. J., Illingworth, G., Franx, M., Kriek, M., & Brammer, G. B. 2010, *ApJ*, 713, 115
 González, V., Bouwens, R. J., Labbé, I., et al. 2012, *ApJ*, 755, 148
 Gonzalez, V., Bouwens, R., Illingworth, G., et al. 2012, *arXiv:1208.4362*
 Kennicutt, R. C., Jr. 1998, *ARA&A*, 36, 189
 Kriek, M., van Dokkum, P. G., Labbé, I., Franx, M., Illingworth, G. D., Marchesini, D., & Quadri, R. F. 2009, *ApJ*, 700, 221
 Labbé, I., et al. 2005, *ApJ*, 624, L81
 Labbé, I., Bouwens, R., Illingworth, G. D., & Franx, M. 2006, *ApJ*, 649, L67
 Labbé, I., et al. 2010, *ApJ*, 708, L26
 Labbé, I., et al. 2010, *ApJ*, 716, L103
 Maiolino, R., Nagao, T., Grazian, A., et al. 2008, *A&A*, 488, 463
 Neistein, E., & Dekel, A. 2008, *MNRAS*, 383, 615
 Oke, J. B., & Gunn, J. E. 1983, *ApJ*, 266, 713
 Oesch, P. A., et al. 2009a, *ApJ*, 690, 1350
 Oesch, P. A., et al. 2010, *ApJ*, 709, L16
 Oesch, P. A., Bouwens, R. J., Illingworth, G. D., et al. 2012, *ApJ*, 759, 135
 Reddy, N. A., Pettini, M., Steidel, C. C., et al. 2012, *ApJ*, 754, 25
 Salpeter, E. E. 1955, *ApJ*, 121, 161
 Schaerer, D., & de Barros, S. 2010, *A&A*, 515, A73
 Schaerer, D., de Barros, S., & Sklias, P. 2012, *arXiv:1207.3074*
 Shim, H., Chary, R.-R., Dickinson, M., et al. 2011, *ApJ*, 738, 69
 Stark, D. P., Ellis, R. S., Bunker, A., Bundy, K., Targett, T., Benson, A., & Lacy, M. 2009, *ApJ*, 697, 1493
 Stark, D. P., Schenker, M. A., Ellis, R., et al. 2013, *ApJ*, 763, 129
 Yan, H., Dickinson, M., Giavalisco, M., Stern, D., Eisenhardt, P. R. M., & Ferguson, H. C. 2006, *ApJ*, 651, 24
 Yan, H., Finkelstein, S. L., Huang, K.-H., et al. 2012, *ApJ*, 761, 177
 Weinmann, S. M., Neistein, E., & Dekel, A. 2011, *MNRAS*, 417, 2737
 Zheng, W., Postman, M., Zitrin, A., et al. 2012, *arXiv:1204.2305*